Effect of Compressive Stress on Electrochemical Performance of Silicon Anodes

Daniela Molina Piper, Thomas A. Yersak, and Se-Hee Lee[z]

Department of Mechanical Engineering, University of Colorado at Boulder, Boulder, Colorado 80309, USA

In this study, we report on the effect that an externally applied compressive stress has on the electrochemical performance of Si anodes. Using the compression of an all-solid-state cell as a convenient format for simulating volume confinement, the electrochemical performance of Si anodes as a function of externally applied compressive stress has been systematically investigated. We verify that the extent of Si lithiation is limited by confining the free volume expansion of nano-Si particles. Volume confinement of Si particles is manifested as an overpotential and results in a stable anode for lithium-ion batteries. These results are foundational and lead to the best understanding to date of the complex electrochemomechanics of a Si-based anode.
© 2012 The Electrochemical Society. [DOI: 10.1149/2.064301jes] All rights reserved.

Si is one of the most promising anode materials for next generation Li-ion batteries because of its natural abundance and its specific capacity in excess of 3500 mAh g^{-1}.[1] To achieve such a massive capacity, it is well known that Si undergoes a volume expansion of roughly 300% accommodating 3.75 mole Li per mole of Si to form Li$_{15}$Si$_4$ at room temperature.[2–4] During volume expansion and contraction, Si particles crack and pulverized fragments can become detached and electrically isolated. The utilization of nano-Si has largely addressed the active material pulverization issue because nanoparticles can better accommodate the large strains associated with lithiation.[5,6] However, expansion of nano-Si particles can also pulverize the composite electrode structure such that electrical contact is lost between active material and conductive additives.[7–11]

The development of a scheme to limit the extent of Si lithiation would improve the cycleability of Si electrodes while only moderately reducing maximum specific capacity. Mechanical confinement provided by an electrochemically inactive matrix or coating to limit the volume expansion of Si may be such a scheme.[12–16] Along these lines, J. Saint et al. observed improved cycleability when nano-Si was coated with a dense carbon matrix.[13] The authors speculated that the mechanical confinement of the nano-Si particles by the carbon matrix enabled the electrode particles to maintain good electrical contact and limited the pulverization of the electrode during cycling. S.-B. Son et al. described a similar outcome as a consequence of the mechanical confinement of nano-Si particles in a Li$_x$Ti$_4$Ni$_4$Si$_7$ matrix.[12] The authors observed that the discharge plateau of their Si-Ti-Ni alloy electrode occurred at a lower potential than that of a Si control electrode. S.-B. Son et al. believe that the overpotential is a manifestation of the internally generated pressure provided by the Li$_x$Ti$_4$Ni$_4$Si$_7$ matrix.[12]

Neither work was capable of characterizing the internally generated stress needed to limit lithiation of Si. Our prior work investigated the performance of nano-Si and μm-Si in a bulk-type all-solid-state cell configuration.[17,18] In order to simulate a condition of volume confinement, we utilize a similar all-solid-state construction and apply a uniaxial external pressure in order to characterize the electrochemomechanics of Si. To the best of our knowledge, no other work has characterized bulk Si electrodes in such a way. Using the cold compression of an all-solid-state cell as a convenient format for simulating volume confinement, we verify that mechanical confinement limits the extent of Si lithiation and is manifested as an overpotential.

Experimental

All processes including synthesis of material, assembly of test cells, and testing of cells were carried out in a dry Argon environment. The 77.5Li$_2$S-22.5P$_2$S$_5$ glass solid-state electrolyte (SSE) used as the basis for our all-solid-state construction is prepared by milling an appropriate ratio of Li$_2$S (Aldrich, 99.999%, reagent grade) and P$_2$S$_5$

(Aldrich, 99%) with a planetary ball mill (Across International PQ-N2). 2 g net weight of material is milled in a 500 mL stainless steel vial (Across International) with two 16 mm diameter and twenty 10 mm diameter stainless steel balls at 400 rpm for 20 hours. The composite electrode is a 1:1:5 weight ratio of crystalline Si powder (50 nm, Alfa Aesar, 98%), copper powder (20–40 nm, Alfa Aesar, 99.9%) and glass SSE, respectively. The composite anode is a vortex mixed 1:4 weight ratio mixture of stabilized lithium metal powder (SLMP, Lectro Max Powder 100, FMC Lithium corp.) and SSE, respectively. A tri-layer pellet, 1.3273 cm^{-2} in diameter, is made by first pressing 200 mg of SSE in the Titanium/Polyetheretherketone (PEEK) die at 1 metric ton. 2 mg of composite electrode and 20 mg of composite anode are then attached to opposite sides of the SSE pellet by pressing at 5 metric tons. Each cell is then uniaxially compressed to a different pressure (3, 150, 230 MPa) that was held constant throughout cell testing. 3 MPa is the typical external pressure applied to cold-compacted all-solid-state test cells to ensure good performance. To apply pressures of 150 and 230 MPa during cycling, we used reinforced cell die clamps, which are similar in design to those used in previous studies (Fig. 1). Electrochemical measurements were carried out using an Arbin 2000 battery test station using a constant current testing scheme to cycle the cells. These electrochemical half-cells were discharged (alloying, lithiation) and charged (de-alloying, delithiation) at 50 μA with a voltage range of 0.01–1.0 V (vs. Li/Li$^+$).

Results and Discussion

Figure 2a presents the cycling capacities of the three cells uniaxially compressed to 3 (blue circles), 150 (red diamonds) or 230 (black squares) MPa. The 3 MPa cell only survives 8 cycles of operation before failure due to an unstable Lithium counter electrode.[19,20] Each cell was cycled at a rate of C/20 to ensure full lithiation of our nano-Si particles. Despite such a slow rate, we find that the initial discharge capacity decreases with an increasing applied pressure. Initial discharge capacities of each cell are circled in yellow. The trend of decreasing initial discharge capacity with increasing applied pressure is highlighted by arrows. The 3 MPa cell achieves a nearly theoretical capacity of 3.7 mole Li per mole of Si while the 150 MPa cell achieves 3 mole Li and the 230 MPa cell achieves only 1.6 mole Li. However, a fraction of the initial capacity must be attributed to the irreversible formation of a solid electrolyte interphase (SEI). A fraction of the nano-Si in the electrode is likely electrochemically inactive because nano-Si particles have a tendency to agglomerate during electrode mixing. With this in mind, the 3 MPa solid-state cell does not achieve a theoretical lithiation despite having an initial capacity of 3.7 mole Li.

The first cycle Coulombic efficiency (CE) for the cell under only 3 MPa of pressure was 55%, while both cells under higher pressure had a first cycle CE of only 40%. Like liquid cells, initial capacity loss in a bulk-type solid-state cell can also be attributed to SEI layer formation. In our case, the SEI will form at the interface between the Si particle
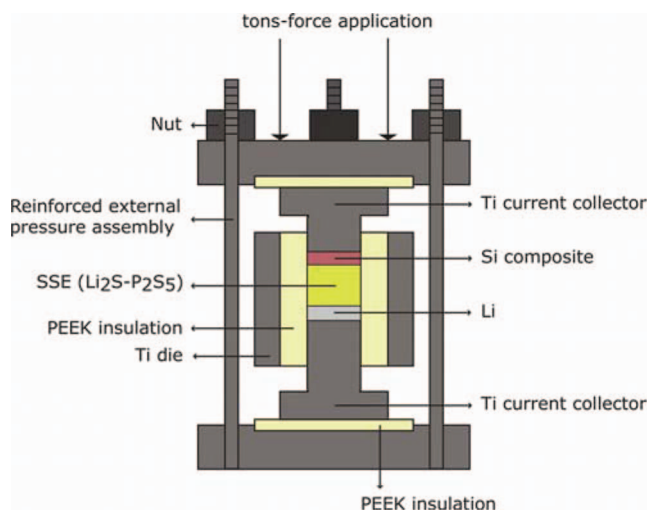
[z]E-mail: sehee.lee@colorado.edu

Figure 1. To apply a large uniaxial external compressive stress, this experiment utilized reinforced Ti/PEEK cell dies. The bulk-type all-solid-state Li battery design is based upon the $Li_2S-P_2S_5$ glass solid-state electrolyte.

and the glass electrolyte. While the composition of the SEI will be different in a solid-state electrode than in a conventional electrode, the effect of first cycle capacity loss is still the same. S.-B. Son et al. have previously identified the SEI of solid-state Si electrodes.[18] To explain the low first cycle CE of the nano-Si electrodes, we must consider the total area of the solid-solid interface between the SSE and Si particles. The Si-SSE interfacial area will be much larger for

Figure 2. (a) Electrochemical performance and CE of solid-state nano-Si composite anodes cycled at a rate of C/20 under compressive pressures of 3 (blue), 150 (red) and 230 (black) MPa. (b) Specific charge (delithiation) capacity retention as a percentage of initial specific capacity.

nano-Si based electrodes than for μm-Si based electrodes. More SEI will initially form in a nano-Si electrode than in a μm-Si electrode. S.-B. Son measured an initial CE of 75% for μm-Si electrodes[18] while our 3 MPa nano-Si electrode has an initial CE of only 55%. The lower CE is due to a larger interfacial area. However, the pressurized 150 and 230 MPa cells have an even lower initial cycle CE of 40%. We can explain the lower CE by considering that the interfacial contact area between Si particles and the SSE particles is further increased under pressure. In order to fully validate this theory more characterization data would be needed; nevertheless, the CEs of the two pressurized cells improve rapidly to match that of the 3 MPa cell.

Figure 2b presents specific charge (delithiation) capacity retention as a percentage of initial specific capacity. The 3 MPa control cell's specific charge capacity (blue) rapidly fades and is only 76.1% reversible by its 8th cycle. However, the 150 (red) and 230 (black) MPa cells quickly stabilize and are 87.3% and 99% reversible by the 21st cycle, respectively. While the application of an external load limits achievable capacity, it also stabilizes the capacity of the cells. Thus, a lower initial capacity is countered by a stable cycling behavior which is an attribute favored for battery materials.

When the voltage profiles of these three cells are studied, we notice that a lower initial discharge capacity is associated not only with an increased externally applied pressure but also with an overpotential (Fig. 3a and 3c). The overpotential observed in Fig. 3 is emphasized with arrows. We expect that the application of pressure will result in better interparticle contact and therefore a decrease in interparticle resistance. However, an increase of bulk and interfacial conductivities would lead to a drop in overpotential, which is not what we observed in our pressurized cells. Therefore, the overpotential observed is dominated by the free volume confinement of Si expansion and not by mechanical contact issues.

The same result is presented as the differential capacity (dQ/dV) of each cells' 1st and 3rd cycle in Fig. 3b and 3d, respectively. Arrows highlight the shift of cathodic (alloying) dQ/dV peaks to lower potentials with the application of a larger external pressure. During the first lithiation (discharge), we observe a voltage plateau at approximately 0.1 V and a corresponding sharp dQ/dV peak. This sharp peak is attributed to the reaction of Li with crystalline Si (c-Si) to form amorphous Li_xSi (a-Li_xSi). Upon subsequent cycles, we do not observe a voltage plateau nor do we observe a sharp dQ/dV peak. Instead, we observe sloping voltage profiles and two broad dQ/dV peaks in both anodic (de-alloying) and cathodic (alloying) regimes. A sloping voltage profile and two broad dQ/dV peaks are consistent with the solid solution reaction of Li with a-Li_xSi.[10] The absence of a cathodic c-Si dQ/dV peak on subsequent cycles indicates the uniform lithiation of electrochemically active nano-Si in our composite electrodes. The absence of an anodic $Li_{15}Si_4$ dQ/dV peak indicates that the crystalline $Li_{15}Si_4$ phase was not nucleated at full discharge. The small diameter of our nano-Si ($\leq$50 nm) particles may have made it thermodynamically unfavorable to nucleate the crystalline phase.[10]

We have shown that the overpotential, or discharge polarization, is related to the mechanical confinement of Si's expansion. During a free volume expansion, Si is allowed to expand unrestricted and no energy is expended for the expansion. The 3 MPa cell approximates this condition because void spaces in the all-solid-state electrode accommodate Si's volume change (Fig. 4a). Our all-solid-state electrodes are formed by cold-compaction without a sintering or densification step so we expect that voids exist between $Li_2S-P_2S_5$ SSE particles.[21] However, these voids are mechanically closed when the all-solid-state electrodes are subjected to large external pressures of 150 and 230 MPa. With the application of a large external pressure, the all-solid-state electrode behaves more like an ideal volume confining elastic matrix.[18] The assumption that the $Li_2S-P_2S_5$ SSE behaves as an elastic matrix is a good one because the electrochemical data presents a reversible system. If the $Li_2S-P_2S_5$ SSE underwent substantial plastic deformation during Si lithiation, then the loss of interparticle contact upon Si delithiation would result in rapid capacity fade. Under a condition of volume confinement, energy is expended to counteract the volumetric strains generated by Si's expansion (Fig. 4b). This energy
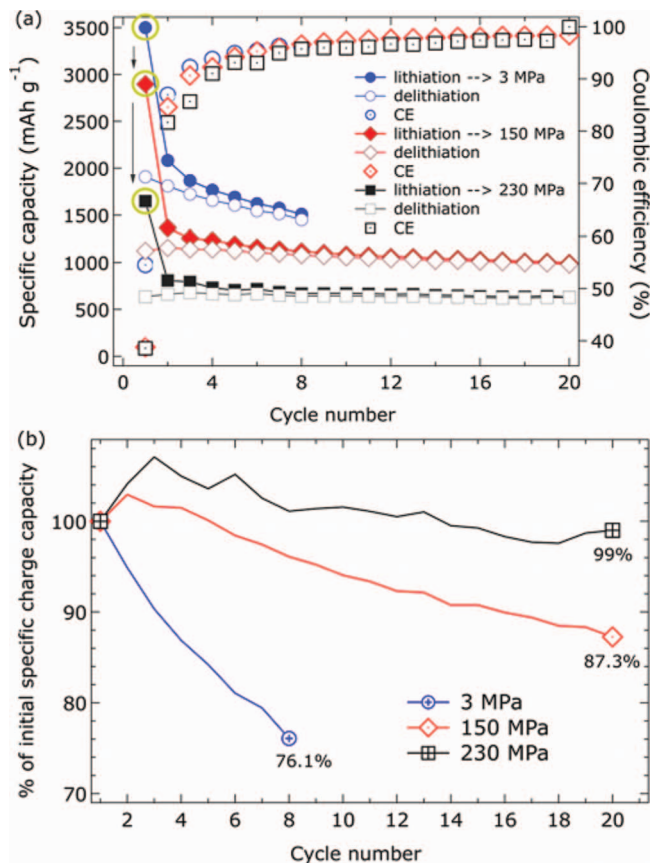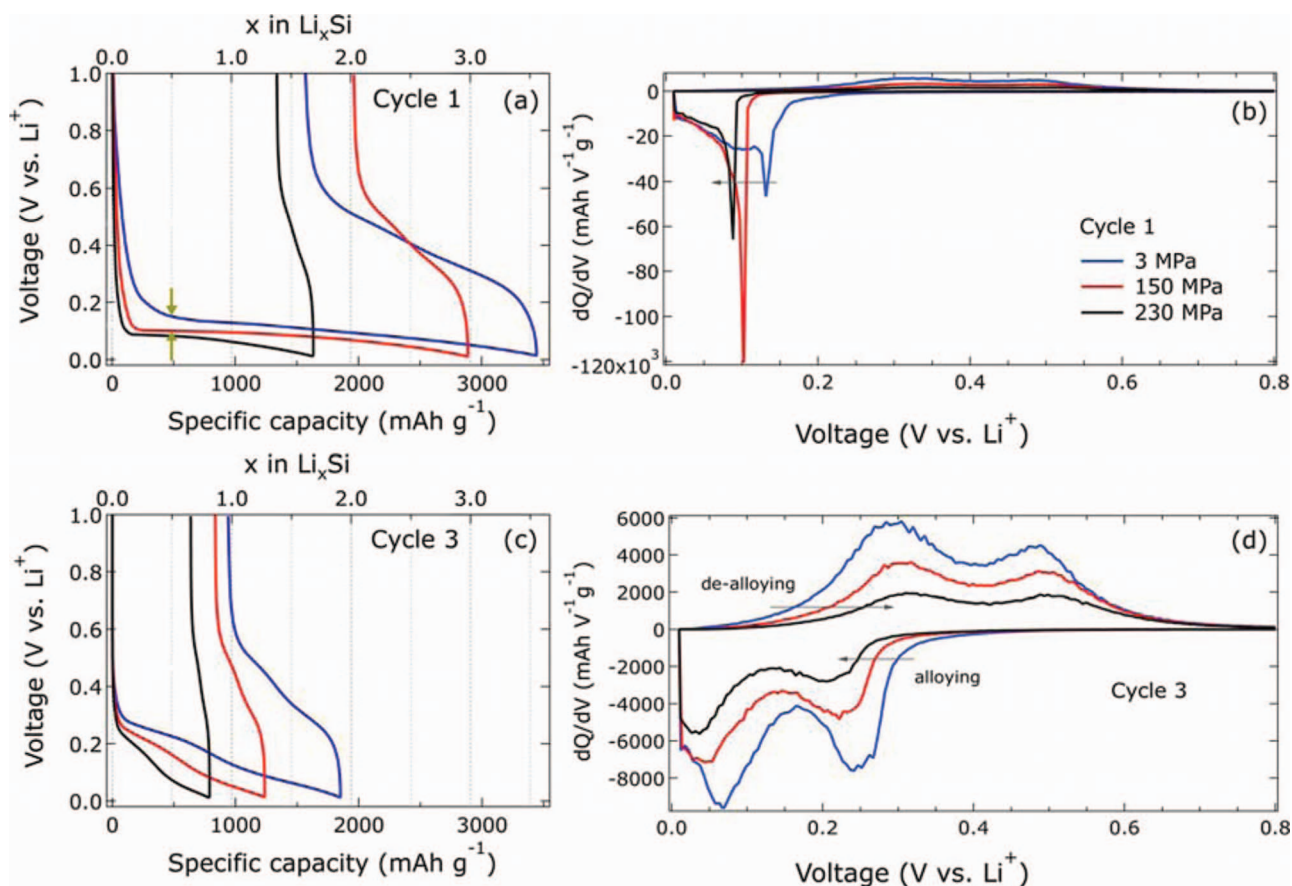
Figure 3. (a) 1st cycle voltage profiles, (b) 1st cycled differential capacity, (c) 3rd cycle voltage profiles and (d) 3rd cycle differential capacity.

expenditure reduces the spontaneity of the reaction and reduces the potential of the initial alloying of c-Si (c-Si → a-Li$_x$Si). At 20% of the initial discharge, the 150 MPa cell exhibits an overpotential of 36 mV and the 230 MPa cell exhibits an overpotential of 50 mV with respect to the 3 MPa cell. After the initial cycle, the solid solution reaction of Li with a-Si (a-Si → a-Li$_x$Si) exhibits a typical sloping profile between 0.3 and 0.01 V. The same overpotential effect is observed in these subsequent cycles as well because the SSE in the composite electrode accommodates Si's volumetric strain elastically.

Under an appropriately large external pressure, our all-solid-state electrode approximates the physics of the previously reported dense carbon coating[13] and Ti$_4$Ni$_4$Si$_7$ matrix.[12] To better understand the behavior of nano-Si expansion in an elastic matrix, we desire to define how the volumetric strain energy increases as a function of Li concen-

tration in Li$_x$Si. We chose to focus our attention on the case of a solid solution reaction between a-Si and a-Li$_x$Si. The results are presented in Fig. 5. Unlike the lithiation of c-Si, the lithiation of a-Si does not result in large structural changes. For this reason, we can apply several simplifications to our analysis: 1) The activity coefficient, γ, of Li in a-Li$_x$Si remains constant with respect to Li concentration, [Li]. 2) The
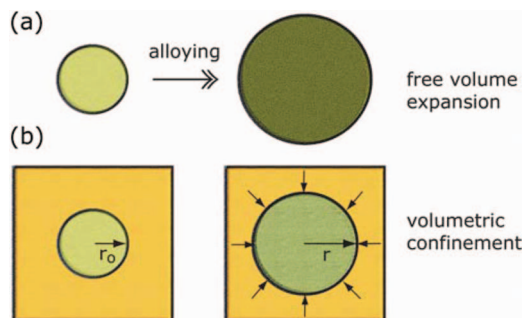

Figure 4. Alloying of a nano-Si particle under a condition of (a) free volume expansion results in full lithiation, while alloying nano-Si under a condition of (b) volumetric confinement in an isotropic elastic matrix results in limited lithiation.
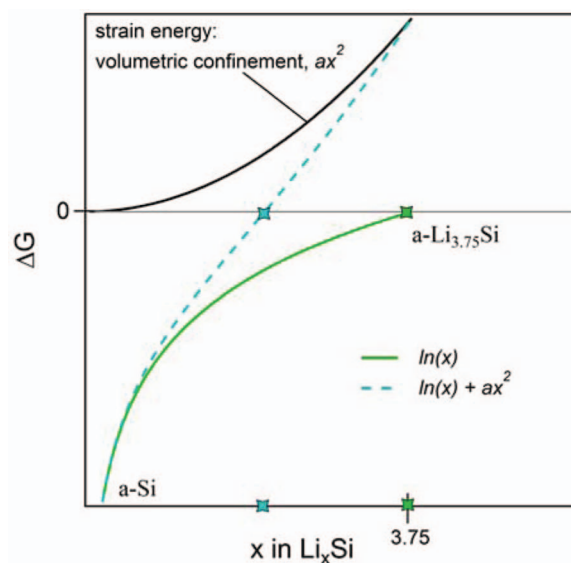

Figure 5. Free energy diagram of the amorphous Si/amorphous Li$_x$Si solid solution under conditions of free volume expansion (solid green), and confined volumetric expansion (dashed blue).

volume of a-Li$_x$Si particle changes linearly with a change in [Li]. The Gibb's free energy of a solid solution reaction follows Eq. 1 where the activity of Li, a$_{Li}$, alloyed in Si is proportional to [Li]. $\Delta G^{0\prime}$ accounts for the standard Gibb's free energy and the activity coefficient of the reaction ($\Delta G^0 + RT ln\gamma$). Under a condition of free volume expansion, the alloying of a-Si will proceed to the room temperature theoretical value of 3.75 mole Li per mole of Si (green solid line). Because our 3 MPa nano-Si electrode achieves a very high capacity and because volume energy will decrease according to r^3 while surface energy will only increase according to r^2, we will neglect the impact that surface energy has on the free energy of nano-Si lithiation.[10]

$$\Delta G = \Delta G^{0\prime} + RT ln\,[Li] \qquad [1]$$

We assume that amorphous nano-Si particles expand isotropically and that the Li$_2$S-P$_2$S$_5$ glass SSE is an isotropic linear elastic solid. As previously mentioned, the sloping voltage profile of our electrodes indicates the solid solution reaction of Li with a-Li$_x$Si. Amorphous materials have no long-range order and therefore no preferential Li transport direction that would cause anisotropic expansion. In this case, the problem simplifies to a state of hydrostatic stress and we consider the bulk modulus of the matrix, K, as a function of volumetric stress, σ, and strain, ε_v, of the Si particle, Eq. 2. Rearranging Eq. 2 we solve for Si volumetric stress as a function of matrix bulk modulus and Si volumetric strain, $\delta V/V$, Eq. 3.

$$K = -\frac{\sigma}{\varepsilon_v} \qquad [2]$$

$$\sigma = -K\frac{\delta V}{V} \qquad [3]$$

In this analysis we do not consider stresses generated inside the Si nano-particle. Here, we are concerned only with the external stress that the expanding Si particle exerts on the matrix, and the equal but opposite stress of the matrix on Si. After substituting the appropriate expressions for volumetric strain, volumetric stress is expressed as a function of unstrained particle radius, r$_0$, and alloyed radius, r, Eq. 4. The integration term in Eq. 4 is strictly a substitution of the δV term in Eq. 3. To ensure a linear elastic treatment of the matrix deformation, it is required that the change in radius is small.

$$\sigma = -\frac{K}{\frac{4}{3}\pi r_0^3}\int_{r_0}^{r} 4\pi r^2 dr = -K\left(\frac{r^3}{r_0^3} - 1\right), r - r_0 \ll r_0 \qquad [4]$$

Finally, volumetric strain energy, U, is given as a function of volumetric stress, Eq. 5.

$$U = \frac{1}{2}\frac{\sigma^2}{K} = \frac{1}{2}Stress \times Strain \qquad [5]$$

With these results it is shown that Li concentration is proportional to volumetric stress according to Eq. 6, 7, and 8.

$$[Li] \propto V \propto r^3 \qquad [6]$$

$$\sigma \propto r^3 \qquad [7]$$

$$[Li] \propto \sigma \qquad [8]$$

Using Eq. 5, it follows that volumetric strain energy is proportional to the square of Li concentration, Eq. 9 and 10.

$$U \propto \sigma^2 \qquad [9]$$

$$U \propto [Li]^2 \qquad [10]$$

[Li] – Lithium concentration in Li$_x$Si
ΔG – Gibb's free energy
ΔG^0 – Standard Gibb's free energy
ΔG$^{0\prime}$ = ΔG^0 + RTlnγ
a$_{Li}$ – Lithium activity in Li$_x$Si
K – Elastic bulk modulus

U – volumetric strain energy
σ – volumetric stress
ε_v – volumetric strain
r$_0$ – initial radius of nano-Si particle
r – radius of nano-Li$_x$Si particle

When the solid solution free energy curve is combined with the parabolic volumetric strain energy curve we obtain a convex curve that achieves equilibrium at a much lower [Li] (Fig. 5, blue dashed line). The coefficient, **a**, of the parabolic profile is influenced by the bulk modulus K; if K increases so will **a**. With this result, we come to the understanding that each incremental increase in [Li] requires a rapidly increasing energy expenditure to elastically deform the matrix in order to accommodate the coincident increase in volume. In this way, the bulk modulus of the matrix can be tailored to achieve a certain degree of Si lithiation. It is important to understand that the experimental trend of decreasing capacity among the 3, 150 and 230 MPa all-solid-state cells is not related to a change in the Li$_2$S-P$_2$S$_5$ SSE's bulk modulus. Instead, this effect is a result of mechanically closing void spaces with the application of external pressure to more accurately simulate complete volume confinement.

The analysis presented here closely approximates any example where Si is embedded in a linear elastic isotropic matrix (i.e. our all-solid-state nano-Si electrodes under large external pressure and Si-Ti-Ni alloys[12]). The physics of thin elastic coatings are much more complex and will require a more detailed approach, though the general conclusions presented here are still relevant. For matrices and thicker coatings, there is opportunity to greatly improve the theoretical analysis by treating the assumptions made in this paper more rigorously. For example, our analysis assumes the linear elastic deformation of the matrix such that the volumetric strain of Si particles is small (i.e. r − r$_0$ ≪ r$_0$). For large volumetric strains, a more rigorous non-linear approach should be taken. Yet, a confined particle may only expand volumetrically by 50% or less such that r is only 14% larger than r$_0$ and our simplified analysis is still valid. An improved analysis may also consider the effects that a compressive stress has on Li$^+$ transport kinetics in Si. Our theoretical analysis only considers the thermodynamic equilibrium of the system. This restricts a direct correlation of our experiments to the theoretical work because the experimental data inevitably includes kinetic polarizations.

Conclusions

S.-B. Son et al. previously reported that their Si-Ti-Ni alloy exhibited an overpotential with respect to a bulk-Si control cell.[12] We observe an increasing discharge polarization with increasing applied external pressure and confirm the hypothesis of S.-B. Son et al.'s study. An all-solid-state electrode under a sufficiently large external pressure confines the volume expansion of nano-Si particles and limits the extent of lithiation. Reducing the extent of nano-Si electrode volume expansion is important if the mechanical pulverization of a composite electrode structure is to be prevented. The application of a pressure, either internally or externally generated, results in a much more stable and long-lasting anode for lithium-ion batteries. Such a stable anode is achieved by sacrificing a fraction of overall capacity. However, total cell specific capacity is not limited by the anode if the anode can achieve a capacity of at least 1000–1200 mAh g^{-1}. Improvements beyond this number result in diminishing returns as far as overall cell specific capacity is concerned.[1] The design of mechanically confining matrixes is therefore an exciting avenue for the development of stable nano-Si anodes.

References

1. U. Kasavajjula, C. Wang, and A. J. Appleby, *Journal of Power Sources*, **163**, 1003 (2007).
2. B. A. Boukamp, G. C. Lesh, and R. A. Huggins, *Journal of The Electrochemical Society*, **128**, 725 (1981).
3. P. Poizot, S. Laruelle, S. Grugeon, L. Dupont, and J.-M. Tarascon, *Journal of Power Sources*, **97-98**, 235 (2001).
4. J. E. Trevey, J. Wang, C. DeLuca, K. K. Maute, M. L. Dunn, S.-H. Lee, and V. M. Bright, *Sensors and Actuators A: Physical*, **167**, 139 (2011).
5. X. H. Liu, L. Zhong, S. Huang, S. X. Mao, T. Zhu, and J. Y. Huang, *ACS Nano*, **6**, 1522 (2012).
6. Y. Oumellal, N. Delpuech, D. Mazouzi, N. Dupré, J. Gaubicher, P. Moreau, P. Soudan, B. Lestriez, and D. Guyomard, *Journal of Materials Chemistry*, **21**, 6201 (2011).
7. R. A. Huggins, *Journal of Power Sources*, **81–82**, 13 (1999).
8. M. N. Obrovac and L. Christensen, *Electrochemical and Solid-State Letters*, **7**, A93 (2004).
9. Y.-M. Chiang, *Science (New York, N.Y.)*, **330**, 1485 (2010).
10. W.-J. Zhang, *Journal of Power Sources*, **196**, 13 (2011).
11. J. H. Ryu, J. W. Kim, Y.-E. Sung, and S. M. Oh, *Electrochemical and Solid-State Letters*, **7**, A306 (2004).
12. S.-B. Son, S. C. Kim, C. S. Kang, T. A. Yersak, Y.-C. Kim, C.-G. Lee, S.-H. Moon, J. S. Cho, J.-T. Moon, K. H. Oh, and S.-H. Lee, *Advanced Energy Materials*, **2**, 1226 (2012).
13. J. Saint, M. Morcrette, D. Larcher, L. Laffont, S. Beattie, J.-P. Pérès, D. Talaga, M. Couzi, and J.-M. Tarascon, *Advanced Functional Materials*, **17**, 1765 (2007).
14. T. Zhang, L. Fu, J. Gao, L. Yang, Y. Wu, and H. Wu, *Pure and Applied Chemistry*, **78**, 1889 (2006).
15. P.-C. Chen, J. Xu, H. Chen, and C. Zhou, *Nano Research*, **4**, 290 (2010).
16. S. Y. Chew, Z. P. Guo, J. Z. Wang, J. Chen, P. Munroe, S. H. Ng, L. Zhao, and H. K. Liu, *Electrochemistry Communications*, **9**, 941 (2007).
17. J. E. Trevey, K. W. Rason, C. R. Stoldt, and S.-H. Lee, *Electrochemical and Solid-State Letters*, **13**, A154 (2010).
18. S.-B. Son, J. E. Trevey, H. Roh, S.-H. Kim, K.-B. Kim, J. S. Cho, J.-T. Moon, C. M. DeLuca, K. K. Maute, M. L. Dunn, H. N. Han, K. H. Oh, and S.-H. Lee, *Advanced Energy Materials*, **1**, 1199 (2011).
19. M. Nagao, A. Hayashi, and M. Tatsumisago, *Electrochemistry Communications*, **22**, 177 (2012).
20. H. Takahara, M. Tabuchi, T. Takeuchi, H. Kageyama, J. Ide, K. Handa, Y. Kobayashi, Y. Kurisu, S. Kondo, and R. Kanno, *Journal of The Electrochemical Society*, **151**, A1309 (2004).
21. H. Kitaura, A. Hayashi, T. Ohtomo, S. Hama, and M. Tatsumisago, *Journal of Materials Chemistry*, **21**, 118 (2011).